Universiteit Utrecht

Faculteit Bètawetenschappen

Density functional theory calculations on the migration of a boron atom adsorbed on a hexagonal boron nitride sheet

Bachelor thesis

G. Buist

Study: Natuur- en Sterrenkunde

Supervisors:

Dr. M.A. van Huis
Drs. R.S. Koster
Debye Institute for Nanomaterials Science, Utrecht University

January 12, 2016

Abstract

DFT calculations were preformed on a single-layer hexagonal boron nitride nanosheet (BNNS) with a boron adatom. Different adsorption sites for the B adatom were investigated and an adsorption site on a B-N bridge site was found to have the highest binding energy. Based on the found adsorption sites a diffusion pathway was found consisting of two hops that would allow the B adatom to move between unit cells. This path was investigated with selective dynamics and the nudged elastic band (NEB) method. The energy barriers of the resulting path turned out to be sufficiently low to allow the B adatom to diffuse throughout the BNNS at room temperature.

Contents

1 Introduction

Developments in nanoscience and the synthesis of new functional materials drive to a great extent technological progress. Often most surprising breakthroughs are made after the discovery of a new material with an unusual complexity or dimensionality. The great amount of attention that two-dimensional crystals have drawn since the first successful synthesis was therefore to be expected. Many scientists have been drawn to those systems in order to discover and make sense of the unusual physical and chemical properties of 2D crystals that may promote novel applications in engineering.[37]

Two-dimensional crystals have a thickness of one up to a few atomic layers and are sufficiently isolated from their environment to be considered free-standing. They can be viewed as atomic planes pulled out of bulk crystals or as unrolled single-wall nanotubes[36]. In comparison with 3D solids, where electron-electron interactions are suppressed, and 1D materials, where phase space strongly constraints these interactions, 2D crystals are characterized by strong quantum fluctuations and an enhanced phase space for interactions[37], giving rise to interesting optical and electronic properties (e.g. single layer of graphene being a zero bandgap semi-metal[35]). 2D crystals may also show different chemical and mechanical behavior compared to 3D solids due to the high (up to infinite) surface-bulk ratio and geometry effects. Graphene for example has a very high thermal conductivity[2], is the strongest measured material[24], can absorb impact very well[26] and is the most impermeable membrane known[3]. New 3D materials may also be created from these 2D crystals via different types of stacking of different 2D crystals.

The first successful isolation of a 2D crystal was graphene which was extracted from graphite via mechanical exfoliation (also known as mechanical cleavage or mechanical peeling)[34]. This method relies on the fact that in graphite in-plane bonds are strong while the layers are weakly coupled via van der Waals interactions. This method was then quickly applied to similar materials such as hexagonal boron nitride (h-BN)[36], which has the same structure as graphite only with alternating B and N atoms in the rings instead of C. Bulk h-BN has captured interest for quite some time due to its high thermal conductivity, low density, electrical insulation, low friction coefficient, great oxidation resistance and excellent inertness. Its 2D equivalent, boron nitride nanosheets (BNNS), posses a unique combination of those properties as well as a much better thermal conductivity, piezoelectric properties, great thermal and chemical stability, extraordinary mechanical strength and resilience, excellent electron emission and strong cathodoluminescence emission in the UV. These properties create a wide range of possible applications for example in compact UV laser devices, as multifunctional composite fillers, dielectric substrates in graphene electronic devices, thermally robust catalytic and sensing substrates, durable field emitters and in biological applications (due to its low toxicity)[32, 39, 40].

Because of their dimensionality 2D crystals have more pronounced changes in their properties due to the adsorption and doping of atoms or molecules and have a much larger surface area available for such reactions (they are essentially gigantic 2D molecules unprotected from the immediate environment) compared to bulk materials. For example the electronic properties of boron nitride nanosheets (BNNS) can be modified by the adsorption of O atoms or organic molecules[9, 47], while adsorbing a C atom on BNNS creates a local magnetic moment of 2.0 μ_B[30] and decorating it and with gold nanoparticles results in excellent catalytic activity for the reduction of H_2O_2[48]. Some 2D crystals are so sensitive to these changes that they can be used as sensors, in fact a graphene sensor has been used to detect the adsorption of single gas molecules[43].

Adsorption reactions can also be used to form new 2D crystals out of initial ones. Examples hereof are graphane and hydrogenated boron nitride nanosheets (BHNH), which can be made by adsorbing hydrogen on graphene or BNNS respectively until they are fully saturated[4, 35]. Because of the large area available for adsorption 2D crystals are useful for storage and capture devices. Good examples are BHNH and graphene with Li and Ca atoms adsorbed respectively, both show great potential for the storage of molecular hydrogen[4, 1]. While graphene adsorbs toxic lead(II) ions from aqueous solutions[13] and BNNS can be used for the reversible capture and release of CO_2[46] as well as the adsorption of pollutant dyes[45, 27]. The possible diffusion of adsorbates on 2D crystals is also of interest since this may lead to the formation of nanoclusters or

self-assembly[38, 49, 14]. When the adsorbates diffuse towards the edges a new 2D crystal may be made at the edge thus creating a heterojunction, which in case of a BNNS graphene heterojunction could be interesting for electronic applications[30]. Thus the possible applications of adatoms on 2D crystals in general and BNNS in specific are quite vast. Therefore the investigation of adsorption sites and diffusion barriers of adatoms on BNNS is of interest.

In this work density functional theory (DFT) calculations were used to investigate the adsorption as well as the migration of a B adatom on a BNNS monolayer. Several adsorption sites were investigated as was the minimum energy path (MEP) for two distinctive hops of the B adatom.

2 Theoretical background

In this section the theoretical background of two methods, density functional theory (DFT) and nudged elastic band method (NEB), as well as the electronic structure problem will be discussed.

2.1 Electronic structure

By solving the electronic structure problem many properties of materials can be predicted, such as bond energies and bond lengths of molecules and adsorbed particles and also lattice structures and physical properties of solids. The ground-state electronic structure problem is defined as finding the ground-state energy of non-relativistic electrons for arbitrary positions of nuclei within the Born-Oppenheimer approximation.[8, 6] The Born-Oppenheimer or adiabatic approximation is done by neglecting the kinetic energy of the nuclei by setting their mass to infinity. This approximation is justified by the observation that nuclei are much heavier than electrons (about $2*10^3$ times heavier) and that thus nuclei react much slower compared to electrons causing them to approximately be fixed points with respect to electrons. This can also be seen by looking at the full hamiltonian for a system of interacting electrons and nuclei eq:1. From that eqation it can be clearly seen how the large nuclei mass (M_I) causes their kinetic term (the one that goes with $\frac{1}{M_I}$) to be small compared to the other terms and that it becomes zero when the mass of the nuclei is set to infinity.

$$H = -\frac{\hbar^2}{2m_e}\sum_i \nabla_i^2 + \sum_{i,I}\frac{Z_I e^2}{|\boldsymbol{r}_i - \boldsymbol{R}_I|} + \sum_{i\neq j}\frac{e^2}{|\boldsymbol{r}_i - \boldsymbol{r}_j|}(\boldsymbol{r}_i) - \frac{\hbar^2}{2M_I}\sum_i \nabla_I^2 + \sum_{I\neq J}\frac{Z_I Z_J e^2}{|\boldsymbol{R}_I - \boldsymbol{R}_J|} \tag{1}$$

After applying the Born-Oppenheimer approximation and by using Hartree atomic units [1], which will be used throughout this section hereafter, the hamiltonian can be written as:

$$H = -\frac{1}{2}\sum_i \nabla_i^2 + \sum_i V_{ext}(\boldsymbol{r}_i) + \frac{1}{2}\sum_{i\neq j}\frac{1}{|\boldsymbol{r}_i - \boldsymbol{r}_j|} \tag{2}$$

Where $V_{ext}(\boldsymbol{r}_i)$ is the potential acting on the electrons due to the nuclei.

2.2 Density functional theory

Density functional theory (DFT) provides a way to treat the problem of many interacting bodies as a much easier-to-solve non-interacting problem. Its methodology is applied in a large variety of fields to many different problems, of which the ground-state electronic structure problem is the most common[7]. In this section the fundamentals, advantages and limitations of DFT in solving the electronic structure problem will be discussed in order to give the reader some familiarity with the theoretical background of this method. First the fundamentals of DFT will be discussed, after

[1] i.e., $\hbar = m_e = e = 4\pi\epsilon_0 = 1$.

that its advantages and lastly some computational details that are of importance in applying DFT on the electronic structure problem.

2.2.1 Kohn-Sham DFT

The basis for modern DFT as used on the electronic structure originates from the papers of Hohenberg-Kohn-Sham [12, 20]. In 1964 Hohenberg and Kohn published a paper in which they formulated density functional theory as an exact theory of many-body systems. Their formulation is valid for any system of interacting particles in a external potential $V_{ext}(\boldsymbol{r}_i)$. This thus includes any problem of electrons and fixed nuclei since the hamiltonian of such a problem can be written as eq.2. For such systems they were the first to prove the following two theorems upon which DFT is based:

First Hohenberg-Kohn theorem[2]**:** *For any system of interacting particles in an external potential $V_{ext}(\boldsymbol{r}_i)$, the potential $V_{ext}(\boldsymbol{r}_i)$ is determined uniquely, except for a constant, by the ground state particle density $\rho_0(\boldsymbol{r})$)*

Second Hohenberg-Kohn theorem:*A universal functional for the energy E[ρ] in terms of the density ρ (**r**) can be defined, valid for any external potential $V_{ext}(\boldsymbol{r}_i)$. For any particular $V_{ext}(\boldsymbol{r}_i)$, the exact ground state energy of the system is the global minimum value of this functional, and the density ρ (**r**) that minimizes the functional is the exact ground state density ρ_0(**r**)*

The first theorem guarantees that given $\rho_0(\boldsymbol{r})$ all properties of the system are determined, via $\rho_0(\boldsymbol{r}) \Rightarrow V_{ext}(\boldsymbol{r}) \Rightarrow H \Rightarrow \Psi(\{\boldsymbol{r}\})$, where $\Psi(\{\boldsymbol{r}\})$ is the wave function of the problem. It doesn't however provide a method to determine the properties of the system directly from $\rho_0(\boldsymbol{r})$. The second theorem guarantees the existence of a functional E[ρ] which can be used to determine the exact ground state energy and density thus solving the ground state electronic structure problem. The only problem is that the exact form of E[ρ] is not known and thus it hasn't got any practical application in this formulation. This changed in 1965 with a new approach by Kohn and Sham which provided a way to make useful, approximate ground state functionals for real systems of many electrons[20]. Their approach was to replace the difficult interacting many-body system with a different and easier to solve auxiliary system. This was an auxiliary system of non-interacting particles ($\Psi(\{\boldsymbol{r}\}) \rightarrow \{\psi_i(\boldsymbol{r})\}$), for which they had the ansatz that the ground state density of this system is exactly equal to the ground state density of the original problem ($\rho_0(\boldsymbol{r}) = \rho_0^{KS}(\boldsymbol{r})$). This so called Kohn Sham system describes the electrons in atoms, molecules and solids as independent particles moving in an effective potential and is thus described by the following eigenvalue problem.

$$H_{KS}\psi_i(\boldsymbol{r}) = \epsilon_i\psi_i(\boldsymbol{r}) \tag{3}$$

With

$$H_{KS} = -\frac{1}{2}\nabla^2 + V_{eff}(\boldsymbol{r}) \tag{4}$$

Moreover they showed that with any given system of many interacting electrons there exists a uniquely defined Kohn Sham system, that is any system of many interacting electron can be mapped to a many body system of independent electrons with an up to a constant uniquely defined V_{eff}. They also defined a general form for the energy functional $E[\rho]$ and the V_{eff} for this

[2]An alternative and more general formulation by Levy and Lieb exists[31, 29, 28]

problem. Both of which are separated in analytically solvable terms and a exchange-correlation term in which all the difficult many body effects of exchange and correlation (XC) are grouped eq:6 and 5. Thus although the Kohn Sham approach involves independent particles it has an interacting density for the DFT.

$$E[\rho(\boldsymbol{r})] = E_{known}[\rho(\boldsymbol{r})] + E_{XC}[\rho(\boldsymbol{r})] \tag{5}$$

In $E_{known}[\rho(\boldsymbol{r})]$ terms representing the independent kinetic energy of the electrons, the Coulomb interactions of the electrons and nuclei, those between pairs of electrons and those between pairs of nuclei are grouped. $E_{XC}[\rho(\boldsymbol{r})]$ is the exchange correlation term.

$$V_{eff}(\boldsymbol{r}) = V_{ext}(\boldsymbol{r}) + V_{Hartree}(\boldsymbol{r}) + V_{XC}(\boldsymbol{r}) \tag{6}$$

Where V_{ext} is the potential caused by the nuclei, $V_{Hartree}$ holds the interaction between pairs of electrons and V_{XC} is the exchange-correlation term which is the functional derivative of $E_{XC}[\rho(\boldsymbol{r})]$:

$$V_{XC}(\boldsymbol{r}) = \frac{\delta E_{XC}[\rho(\boldsymbol{r})]}{\delta \rho(\boldsymbol{r})} \tag{7}$$

Also since this system consists of independent particles the electron density obeys the following equation:

$$\rho(\boldsymbol{r}) = \sum_i |\psi_i(\boldsymbol{r})|^2 \tag{8}$$

In conclusion if $E_{XC}[\rho(\boldsymbol{r})]$ is known the Kohn Sham eqations(3) become a self-consistent computational problem whose solution is the solution to the the electronic structure problem of the interacting system. In Fig.1. it is outlined how such a calculation would work. However $E_{XC}[\rho(\boldsymbol{r})]$ isn't known exactly although different approximations exist which are precise enough to be of practical use. The choice for such an approximation will be discussed in section2.2.3.

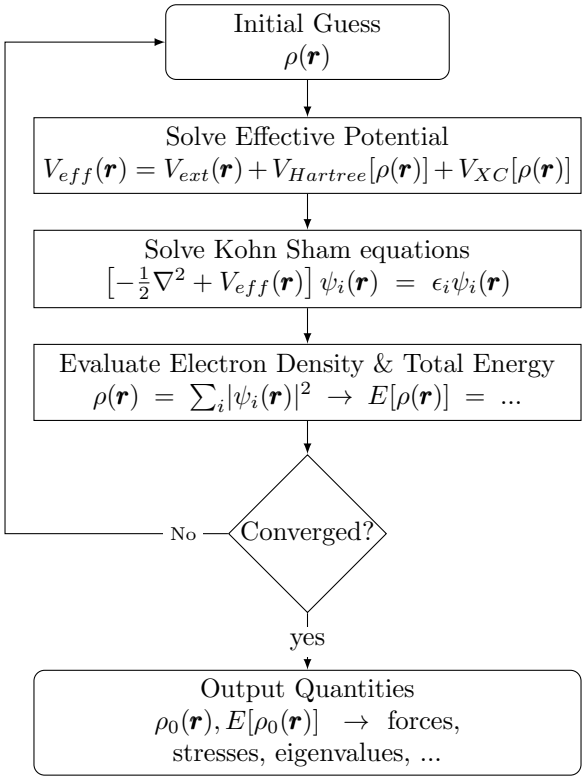

Figure 1: Flow chart of the Kohn Sham iteration procedure. First an initial guess for the electron density is made, which is used to determine the effective potential. This in turn enables to solve the Kohn Sham equations. Then the electron density and the total energy can be calculated which subsequently can be compared to the initial guess values. If they differ a new value for the density is chosen and the process repeats until self-consistency is reached. When this is reached the electronic structure of the system is solved and various physical quantities, such as the forces on the ions, can be calculated or estimated.

2.2.2 Why DFT?

DFT has two big advantages, which Kohn clearly explains in his Nobel lecture[23], the first is conceptual. Instead of focusing on 3N-dimensional[3] Hilbert space of single-particle states, it deals with physical quantities defined in the three-dimensional coordinate space, of which the most common and fundamental is the electron density $\rho(\boldsymbol{r})$. As the size of the system increases and the number of electrons becomes enormous a description of the system in terms of single particle wave functions becomes increasingly hard to comprehend especially when a high accuracy is required for which an increasing amount of exited or "virtual" orbitals are necessary. Whereas quantities on which DFT focuses, such as $\rho(\boldsymbol{r})$, are much easier visualized for very large systems, thus DFT gives a useful and complementary look from a different perspective.

The second advantage is practical. Because of the form of the Kohn Sham equations (3) the computational costs of solving the problem with DFT scales with N. While wave function methods scale much more quickly with system size, for example Hartree Fock calculations scale with N^4 while post-Hartree Fock methods scale with $N^5 \sim N^8$. Thus the computation costs of wave function methods become impractically large quite quickly compared to DFT. As such DFT methods are necessary to preform electronic structure calculations on large systems such as large molecules and solids in a reasonable amount of time.

[3]N being the amount of electrons and every electron having 3 spatial dimensions

2.2.3 Computational details and accuracy

In this section the computational details, such as choice of exchange-correlation functional, will be discussed in order to provide the reader with the information necessary to reproduce the results.

Exchange-correlation functional The reliability of the results of DFT calculations depend to a great extent on which approximation for the exchange-correlation functional is used. As such much effort has been put in developing more precise functionals resulting in a wide range of such functionals. These functionals all have their own advantages and are thus suited for different problems, the B3LYP[25] is for example popular with chemist but it preforms more poorly for extended systems such as crystals. For such systems the general gradient approximation functional proposed by Perdew, Burke and Ernzerhof (PBE or GGA-BPE)[42] provides good results and is widely used. Since the system of interest in this work has a crystal structure the PBE functional was used for all calculations.

Dispersion correction Dispersion forces, also known as London or van der Waals forces have always posed a problem for standard DFT functionals [15, 16]. This is because these interactions cause long-ranged/non-local correlations while standard approximations for E_{XC} are local. As such in systems where these attractive forces are for a large part responsible for the bonds the binding energy/bond strength ends up being underestimated by DFT. The adsorption of particles on a surface can be achieved through van der Waals force, when this is the fundamental interacting force it is called physisorption. Thus to get correct results including corrections to account for dispersion interactions are necessary. In this work these were done by a van der Waals functional made by Klimeš[19, 18].

Basis set and core electrons The Kohn Sham wave functions from eq;3 can be represented in terms of any complete basis set[17]. For periodic systems it is most useful to expand the wave functions in the form of a plane-wave basis set (eq:9). Therefore all calculations done in this work were carried out using the plane-wave basis.

$$\psi_{i,\boldsymbol{k}}(\boldsymbol{r}) = \sum_{\boldsymbol{G}} c_{i,\boldsymbol{k}}(\boldsymbol{G}) exp[i(\boldsymbol{k}+\boldsymbol{G})\cdot\boldsymbol{r}] \tag{9}$$

Here we however run in some practical implications since the summation in eq.9 is over all reciprocal lattice vectors G, which means that G has an infinite amount of possible values. But since plane-waves can be seen as solutions to the Schrödinger equation with a kinetic energy $E = \frac{\hbar^2}{2m}|\boldsymbol{k}+\boldsymbol{G}|$ and since lower energies are physically more significant than higher energies the wave function can be reasonably be approximated by truncating the expression at a high enough energy. For higher cutoff energies the wave functions become more accurate while the computational cost increases. In order to find a high enough cutoff energy for any specific some initial calculations need to be done, these can be found in the appendix (A.1), for the system investigated in this work a cutoff energy of 750 eV was found to be sufficient[4]. It is important to note that a cutoff energy of 750 eV is only sufficient in combination with the projector augmented wave method (PAW)[5] of Blöchl, which is used to describe electrons near ion cores, with an energy cutoff of 1050 eV for the augmentation charges. Without the PAW method a much larger energy cutoff is needed for the plane-waves in order to describe the rapidly oscillating electrons near ion cores. By using the PAW method and a lower cutoff energy for the plane-waves the computation costs are reduced.

k-point sampling in the Brillouin zone For DFT calculations done with a plane-wave basis set for many calculations the integral in eq.10 has to be evaluated.

$$I = \frac{V_{cell}}{(2\pi)^3}\int_{BZ} g(\boldsymbol{k})d\boldsymbol{k} \tag{10}$$

[4] a convergence within 1 meV/atom was considered sufficient

Here V_{cell} is the volume of the unit cell, $g(\boldsymbol{k})$ is a generic function of k vectors and it is integrated over all possible values of $\boldsymbol{k}$ in the Brillouin zone. This is an infinite-dimensional problem and thus needs to be evaluated numerically with a discrete set of properly weighted k-points. In order to efficiently do this a method was developed by Monkhorst and Pack[33]. Within most simulation packages including the package used for all calculations in this work, the Vienna ab initio simulation package (VASP)[22, 21], this method is an option and only the amount of k-points in every direction needs to be specified. The accuracy and the computational cost of the DFT calculations increase with the density of k-points sampled in the Brillouin zone. Thus just as with the cutoff energy some preliminary calculations need to be done to find a sufficient value for the k-point density, see appendix (A.1). It is also important to note that for increasing cell volume in real space the Brillouin zone in reciprocal space decreases thus reducing the k-point sampling density needed for good results. Throughout this work following the method of Monkhorst-Pack k-space was sampled with a Γ centered Monkhorst-Pack grid with a k-point mesh of 2x2x1, this ensured an energy convergence within 1 meV/atom

2.3 Nudged elastic band method

Although with DFT local energy minima and thus adsorption sites can be calculated quite easily on its own it isn't very well equipped to determine transition states and find the minimum energy pathway (MEP) between two local energy minima. A method made to find these MEPs between a stable initial and final state and that is widely used in DFT calculations is the nudged elastic band (NEB) method. With the NEB method a string of images (geometric configurations of the system) is used to describe a reaction pathway between the initial and final state. The initial pathway is usually made via a linear interpolation between the initial and final state, although with some problems a different setup is better. Then the images along the NEB are relaxed to the MEP via a scheme were the potential forces only act perpendicular to the band and artificially added spring forces act along the band. So for every image i the force on it has the form of the equation 11. Where $F_i^{\perp}$ is the part of the force which the system exerts on the image perpendicular to the path and $F_i^{\parallel}$ is the artificially added spring force acting along the path.

$$F_i^{NEB} = F_i^{\perp} + F_i^{\parallel} \tag{11}$$

By iteratively adjusting the images/configurations of the NEB until the $F_i^{\perp}$ becomes zero the NEB is slowly adjusted until it forms the MEP. In NEB calculations it is important to determine for every image the tangent, $\hat{\boldsymbol{\tau}}_{\boldsymbol{i}}$ along the band in order to calculate the correct components of F_i^{NEB}. There are several ways to do this but the upwind tangent method as described by Henkelman *et al.*[10] gives the best stability and avoids the development of artificial kinks along the path at high force regions. This is why although VASP comes with a built in NEB method for the NEB calculations a package developed by the Henkelman group was used[10, 11, 44]. On a side note because for a NEB one needs to run DFT calculations for all the images at once the computation cost of a single calculation can become quite high. Also the Henkelman package comes with a climbing image method which assures that an image ends up at the saddle point, but since the saddle point was the already known final state this method was turned off. Finally NEB calculations are local not global optimization calculations, i.e. it minimizes to a local not global MEP. So a NEB calculation can give accurate information about a particular transition but it can not indicate whether other transitions, with a lower energy barrier, exist related to the same initial and final states. For example to move an adatom from one adsorption site to another can happen via said adatom simply moving over the surface, but another way of achieving this is via the exchange mechanism where the adatom replaces an atom of the same species in the surface layer while the surface atom pops up onto the surface in a different location becoming an adatom. Both of them have the same result but the MEPs are different.

3 Computational setup

In this section the specific model and setups used for the calculations will be described.

3.1 Supercell

As noted in section 2.2.3 all calculations in this work were done using the Vienna ab initio simulation package (VASP)[22, 21]. In order to simulate a crystal this package needs a so called supercell as input which is then periodically repeated in the three spatial directions. The size and shape of the supercell as well as the number, elements and positions of the atoms in the supercell have to be specified in order to create the supercell. Since the system of interest is 2D hexagonal boron nitride with a single adatom it is important to create a supercell in such a way that the adatoms in different periodic images don't interact with each other as well as that images stacked in the z-direction don't interact with each other at all. In order to achieve this a supercell with a vacuum layer greater than 20 Å and a horizontal width of at least 13 Å was created. the h-BN sheet was found to have a lattice constant of 2.51 Å, see appendix (A.2), which leads the supercell to be filled with 36 atoms of nitrogen and boron each to create the BNNS plus an extra atom as adatom, see fig.2.

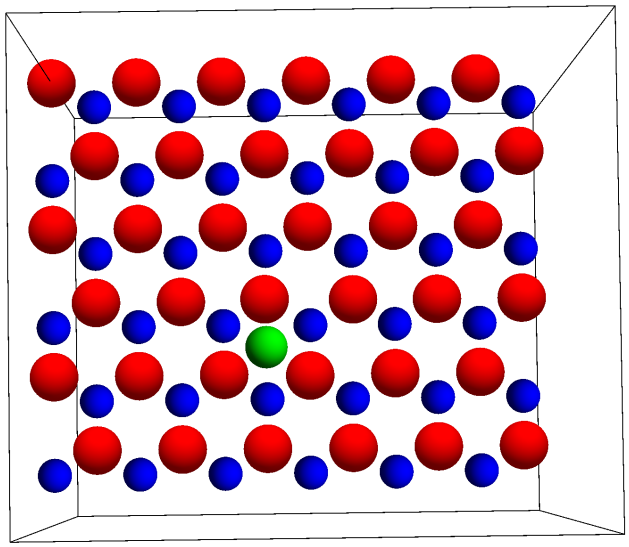

Figure 2: Top view of an example supercell with a BNNS (boron and nitrogen atoms red and blue respectively) with an adatom (green).

3.2 Adsorption sites

In order to determine the adsorption sites of an adatom several calculations were done with different initial guesses on which ionic relaxation was applied in order to find the adsorption position with the lowest total energy and thus with the highest bond strength/energy. In the scheme of fig.1 V_{ext} is not updated during the loop and thus the positions of the ions is not updated. As such this scheme can not be directly used to relax the ionic structure, but after the electronic relaxation the forces on the ions can be calculated. These forces can then be used as initial input for a different algorithm that will update the ion positions. This results in a new V_{ext} which is used for a new electronic relaxation which will provide the ionic relaxation algorithm with new input.

Within the VASP package various ionic relaxation algorithms are provided the one used throughout this work was the RMM-DIIS algorithm from VASP. Six different positions where used as initial guesses (fig.3), the sites on top of a boron/nitrogen atom (B/N TOP), in the center of the hexagonal unitcell (H6), between a boron-nitrogen pair (B-N or hetero bridge), between a boron pair (B-B or B-bridge) and between a nitrogen-nitrogen pair (N-N or N-bridge). For these two different types of relaxations, electronic and structural, different convergence criteria were used, for the electronic relaxation the energy difference needed to be within 10^{-5}eV to be considered converged while for the structural relaxation 10^{-4}eV was used as convergence criterium.

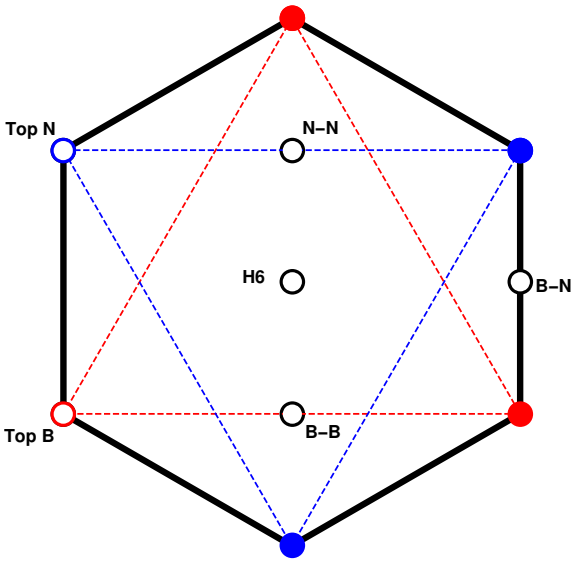

Figure 3: A unitcell of hexagonal boron nitride with the six different trial positions of the adatom; in the middle of the hexagon (H6), on top of an N atom (Top N), on top of an B atom (Top B), equidistant from an N and an B atom or hetero bridge (B-N), equidistant from two N atoms or N-bridge (N-N) and equidistant from two B atom or B-bridge (B-B). B atoms are red while N atoms are blue.

3.3 Migration

In section 2.3 the NEB method with which the MEP can be determined was discussed, but because of its computational costs an other method to determine the migration path of an adatom was also implemented which will be discussed here. VASP comes with the option of selective dynamics with which the position of arbitrary atoms can be fixed in any of the directions of the 3 vectors used to define the supercell. In order to determine the transition states between two adsorption sites a number of adatom positions between them are generated through interpolation just as with the NEB method. But instead of running one simulation with all of these positions within the h-BN crystal a seperate DFT calculation is run for each position in which the position of the adatom is kept fixed in one direction along the BNNS surface while a structural relaxation is done. Because the supercell for all these calculations was orthogonal the adatom is only relaxed with respect to its height and the direction along the BNNS that is perpendicular to the direction in which the adatom is fixed. This way the adatom is driven towards a position which minimizes the energy without being able to "fall" back to the adsorption site. Thus by running serveral of these calculations a number of intermediate positions between two adsorption sites can be determined. While running these selective dynamics calculations all the atoms along two of the edges of the supercell were kept fixed in all directions. This was done in order to prevent all the atoms of the BNNS to move the same distance as the adatom was moved which would effectively return the arrangement in which the adatoms is on the adsorption site.

4 Results and Discussion

4.1 Adsorption sites

In table 1 the adsorption energies of the trial adsorption sites can be found. The adsorption energy, E_{ad} was defined as;

$$E_{ad} = E_{atom} + E_{BNNS} - E_{system} \tag{12}$$

Where E_{atom} is the energy of a single adatom, E_{BNNS} is the energy of a perfect BNNS without a adatom and E_{system} is the energy of the system of BNNS with an adatom on it.

Table 1: Adsorption energies of the adsorption sites, for each species of atom a comparison of the energies of the adsorption sites with the lowest energy adsorption site and the distances between the adatoms and the BNNS.

Atom species	Site	ΔE (eV)	adsorption energy (eV)	height adatom (Å)
B	Center	0.406	0.335	2.74
	Hetero bridge	0.000	0.742	1.83
	B brigde	0.117	0.625	1.81
	N bridge	0.192	0.550	2.03
	on B	0.420	0.321	2.80
	onN	0.116	0.626	1.81
N	Center	2.352	0.579	2.26
	Hetero bridge	0.000	2.931	1.63
	on B	1.295	1.636	1.88
	onN	0.021	2.910	2.78

From the table it can found that the hetero bridge site for both the N and B adatom has the lowest energy which leads to that site being the most favorable for adsorption. The adsorption energy of the N adatom for this site is about 4 times greater than that of the B adatom making the adsorption of a N atom more favorable than the adsorption of a B atom. Also the adsorption of an N atom on top of an atom in the BNNS caused a vertical displacement in the position of that atom. When adsorbed on top of a B atom the B atom moved closer ('upwards') to the adsorbed N atom. While when it was adsorbed on top of an N atom the N atom in the BNNS moved away ('downwards') from the adsorbed N. The distance between the B atom on which N was adsorbed and the BNNS was 0.39 Å ('upwards') and for the N atom of the BNNS 0.91 Å ('downwards'). For a adsorbed B atom such displacements were not present. Although the adsorption sites in table 1 are named after their trial positions, not all adsorption sites remained the same after the ionic relaxation. In fig.4 the adsorption sites that were found after the relaxation are shown.

In fig.4b it can be seen that the initial guesses for the adsorption sites of an N atom were quite good and that only the position for the hetero brigde site was moved slightly closer to the N atom in the BNNS. In fig.4a however only the center and on B trial sites turned out to be actual adsorption sites for an B adatom. For the N-bridge trial position the B adatom was moved closer to the B atom in the BNNS while for the hetero brigde position it was moved closer to the N atom reducing the horizontal distance between them from $\frac{1}{2}$l to about $\frac{1}{3}$l, where l is the distance between a B and N atom in the BNNS. Lastly for B-bridge trial site the B adatom was moved closer to the N atom while for the on N trial site it was moved closer to the B-bridge position. The result is that their respective found adsorption sites are very close to each other and since their adsorption energies are almost equal the resulting found adsorption site for those 2 calculations can be considered the same.

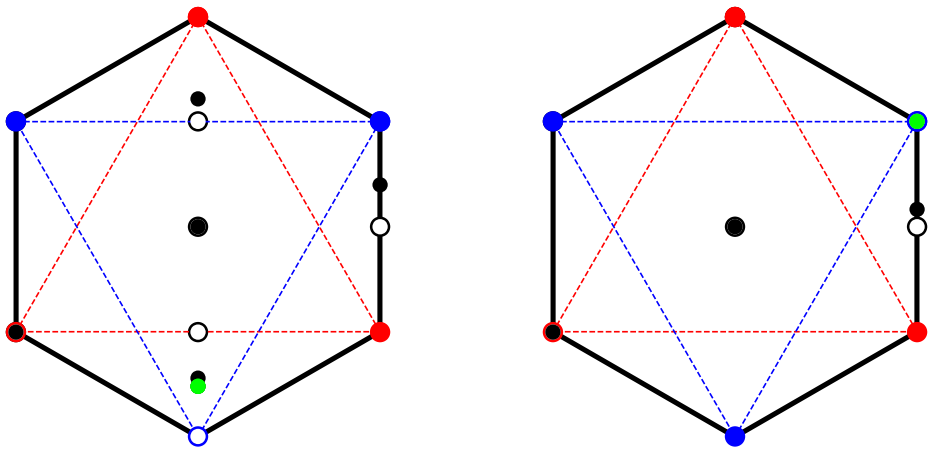

(a) (b)

Figure 4: The trial adsorption sites are indicated by white circles, the found adsorption sites are indicated by black circles. In (a) the found adsorption sites for an adsorbed B atom are shown and in order to distinguish between the found adsorption site for on N and the B-bridge trial sites the adsorption site for on N is indicated with a green circle. In (b) the found adsorption sites for a N adatom are shown with the on N adsorption site shown in green in order to make it clearly visible

4.2 Migration path

Based on the adsorption sites found for a B adatom a likely migration path between unit cells was constructed. This path consisted of two parts, a short path where the B adatom moved from a hetero bridge site around a N atom likely via a on N site to another hetero brigde site and a long path where the B adatom moved from a hetero brigde site around a B atom likely via the N-bridge site to another hetero brigde site. First the results for the short path around the N atom will be discussed, after which the same will be done for the long path around the B atom and lastly those results are combined into a single path that enables migration of the B adatom throughout the BNNS.

4.2.1 Migration path around nitrogen

Since the path around N was short both the NEB and selective dynamics (SD) method could be used. Both methods showed a negligible amount of change in the distance between the BNNS and the B adatom during its migration around the N atom. With the NEB method the change in distance stayed within the range of 0.03 Å while for SD it was within the range of 0.05 Å. The resulting path along the BNNS, shown in fig.5, however differed greatly between both methods as can be seen in fig.6.

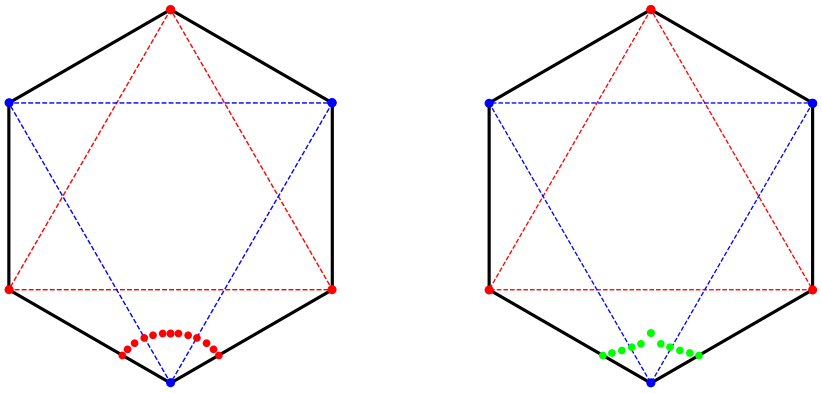

(a) (b)

Figure 5: Migration path of a B adatom around N in a hexagonal unit cell of boron nitride calculated with the NEB method (a). Migration path of a B adatom around N in a hexagonal unit cell of boron nitride calculated with SD (B).

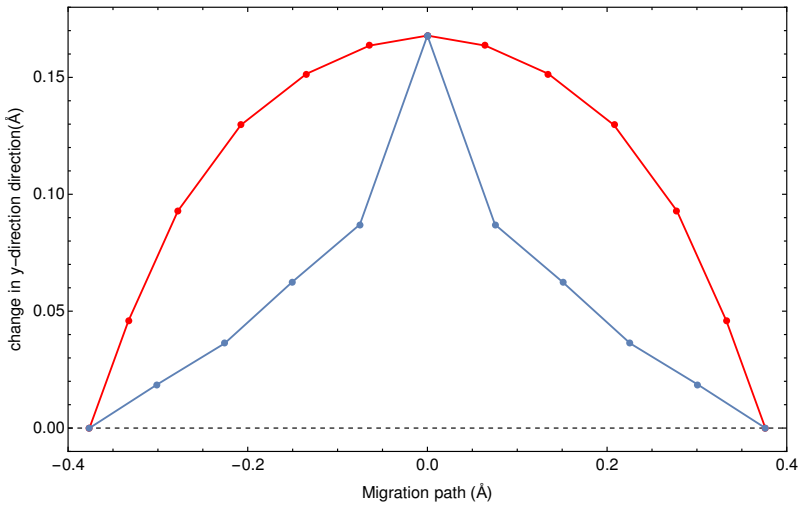

Figure 6: Migration path of a B adatom on h-BN around a N atom calculated with the NEB method (red) and with selective dynamics (blue). The origin was set at the position of the N atom. The lines were drawn to guide the eye.

The energy change during the migration from hetero bridge to hetero bridge around an N atom calculated by both methods is shown in fig.7. The methods give a different shape for the energy change during the migration but have their peaks are equal in height at have the same position. This is because although the migration paths calculated with both methods are different they both go trough the adsorption site found with the on N trial site.

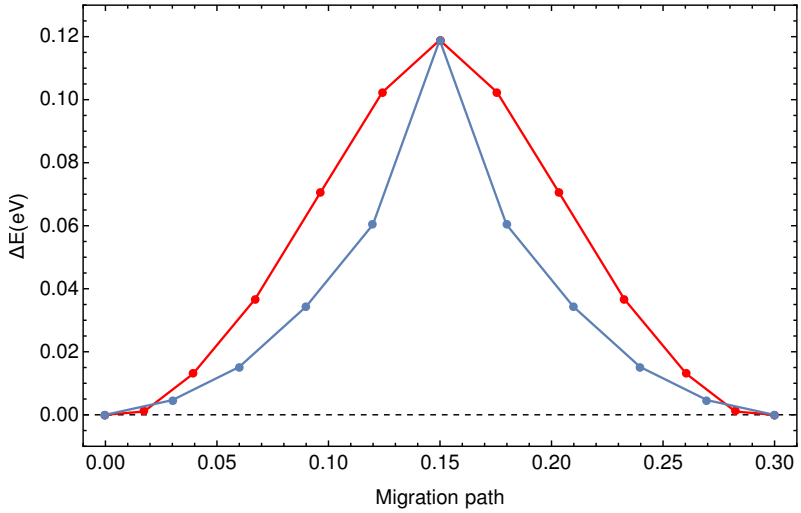

Figure 7: Energy increase during the migration of a B adatom around a N atom calculated with the NEB (red) and SD (blue) methods. The migration path is expressed in its fraction of the total path of moving around an N atom and a B atom. The lines were drawn to guide the eye

4.2.2 Migration path around boron

For the long path around the B atom only the selective dynamics method was used since it required too many images for the NEB method. In the direction along the BNNS and perpendicular to the direction in which the B adatom was fixed (y-direction) the B adatom showed a negligible change, within a range of 0.04 Å, in position during its migration around the B atom. The movement of the B adatom along the BNNS can be seen in fig.9. How the distance of the B adatom to the BNNS changed during the migration around the B atom can be seen in fig.8.The change in energy during the migration of the B adatom around the B atom is shown in fig.10.

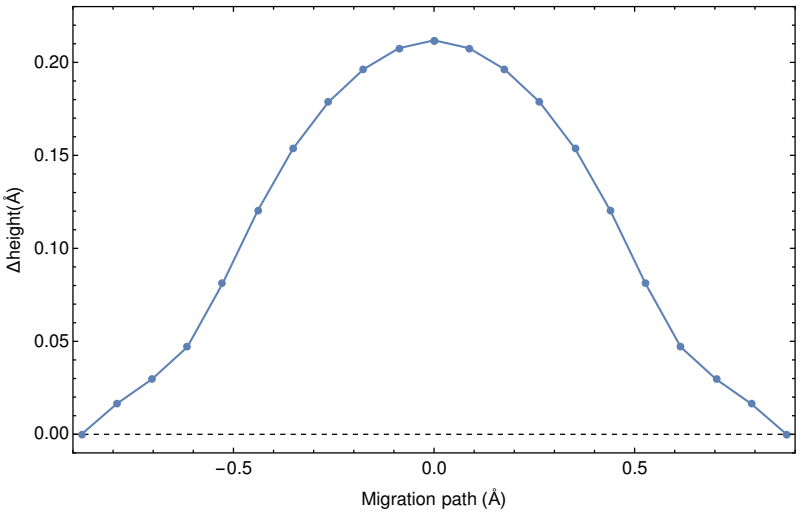

Figure 8: Change in distance between the B adatom and the BNNS during the migration of the B adatom around the B atom. The path is taken in the direction in which the B adatom was fixed and the boron atom around which it moves is located at 0. The lines were drawn to guide the eye.

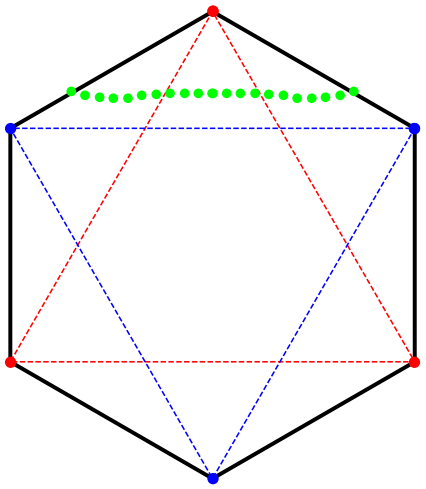

Figure 9: Migration of a B adatom around a B atom in a hexagonal boron nitride unit cell.

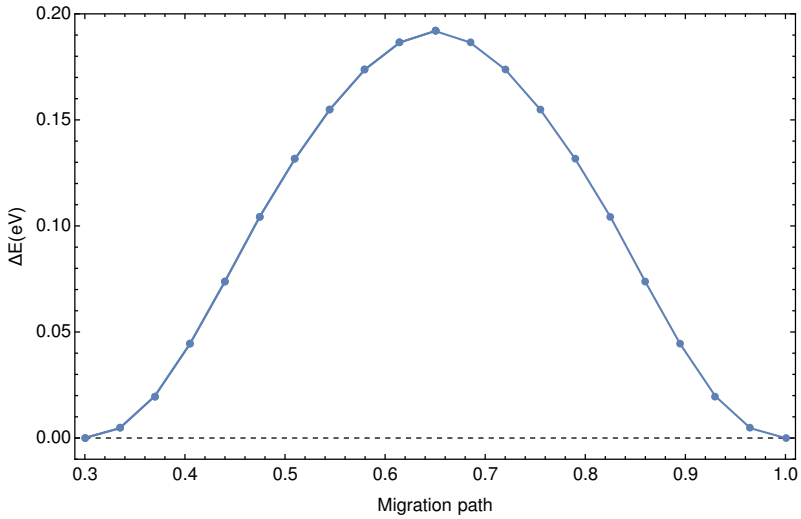

Figure 10: Energy increase during the migration of a B adatom around a B atom calculated with SD. The migration path is expressed in its fraction of the total path of moving around an N atom and a B atom.

4.2.3 Total migration path

By combining the migration paths of the B adatom around the N atom and the one around the B atom a new migration path is constructed which allows the B adatom to move to a neighboring unit cell (fig.12) or it can make a turn within the unit cell, fig.11. The change in energy during the migration is shown in fig,13.

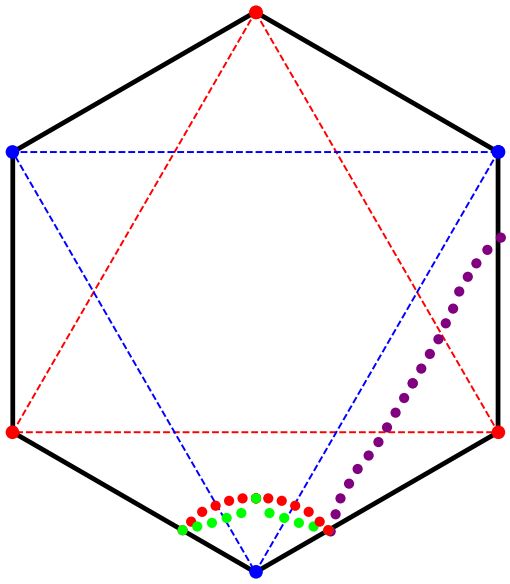

Figure 11: The migration of a B adatom in a hexagonal unit cell of boron nitride. Red is migration around a N atom calculated with the NEB method, green the SD around a N atom and purple the SD around a B atom

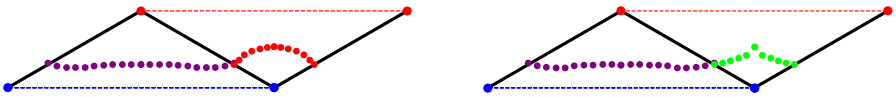

(a) (b)

Figure 12: Migration to a neighboring unit cell with the migration around a N atom calculated with the NEB method (a) and with SD (b). The migration around the B atom is calculated with SD and is indicated by purple, green is the migration around a N atom calculated with SD and red is around a N atom calculated with the NEB method.

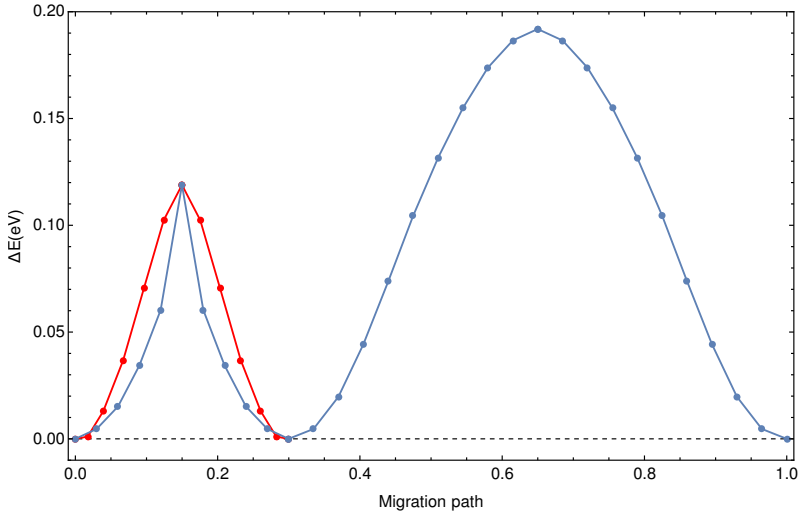

Figure 13: The change in energy during the migration of a B adatom around a N atom first and a B atom second. Red indicates the calculations done with the NEB method and blue with SD. The lines were drawn to guide the eye.

4.3 Diffusion of B adatom

With the energy landscape known some calculations on the kinetics of the B adatom can be done. The jump rate of a adatom jumping from one hetero bridge site to another is described by equation 13.

$$\Gamma = \nu_0 e^{-E_{diff}/(k*T)} \tag{13}$$

Where Γ is the jump or hopping rate, ν_0 is the vibrational frequency of the adatom which is typically around 10^{13}Hz, E_{diff} is the height of the energy barrier, k is the boltzman constant and T is the temperature. In order for diffusion to happen E_{diff} has to be smaller than the adsorption energy otherwise desorption will be the dominant process. Since the peaks in the energy curve of the diffusion path are the on N site and N-bridge site both peaks are lower than the adsorption energy of the hetero bridge site (see table 1). Since the diffusion path consists of two different hops which leads to two different energy barriers two hopping frequencies can be defined. Γ_1 for the small energy barrier E_1 which needs to be overcome for a hop around a N atom and Γ_2 for the larger energy barrier E_2 which needs to be overcome for a hop around a B atom. Since E_2 is larger than E_1, Γ_2 is larger than Γ_1 at equal temperature. Thus three regimes can be defined, one where the T is so low that both the hop around a N atom and the hop around a B atom can not be made ($\Gamma_2 < \Gamma_1 << 1$). A temperature regime where the B adatom can hop around a N atom but not around a B atom ($\Gamma_2 << 1 < \Gamma_1$) and thus the B adatom is trapped on the three hetero bridge sites around one N atom. The last regime is when T is so high that the B adatom

can hop around both the N atom and the B atom ($1 < \Gamma_2 < \Gamma_1$) and thus the paths in figures 12 and 11 are accessible. In the table below the hopping frequencies for the two energy peaks has been calculated for different T.

Table 2: Hopping frequencies for diffusion around a N atom (Γ_1) and around a B atom (Γ_2) for different temperatures.

Temperature (K)	$k*T$ (eV)	Γ_1 (s^{-1})	Γ_2 (s^{-1})
30	0.003	$1.06 * 10^{-7}$	$5.78 * 10^{-20}$
50	0.004	10.3	$4.54 * 10^{-7}$
80	0.007	$3.23 * 10^{5}$	8.14
100	0.009	$1.02 * 10^{7}$	$3.57 * 10^{6}$
150	0.013	$1.01 * 10^{9}$	$1.46 * 10^{8}$
200	0.017	$1.01 * 10^{10}$	$1.35 * 10^{9}$
273	0.024	$6.38 * 10^{10}$	$2.87 * 10^{9}$

From the values of table 2 it is clear that at room temperature the B adatom can diffuse throughout the BNNS. From the hopping frequency it is possible the calculate the average distance traveled by a B adatom after a time t with the following equation.

$$\sqrt{\langle \Delta r^2 \rangle} = a\sqrt{\Gamma t} \tag{14}$$

Where a is the distance traveled by a hop and t is the time. This equation does not account for a path with different kinds of hops but from table 2 and fig.14 it can be seen that when Γ_2 is large enough to allow hopping, Γ_1 is much larger than Γ_2 which makes an approximation whereby only Γ_2 is taken into account reasonable. Considering a, the hop around a N atom and the hop around a B atom add up to a path with the length of the lattice constant, thus a=2.51 Å. With this the average distance traveled for different temperatures can be plotted against time as done in fig.15.

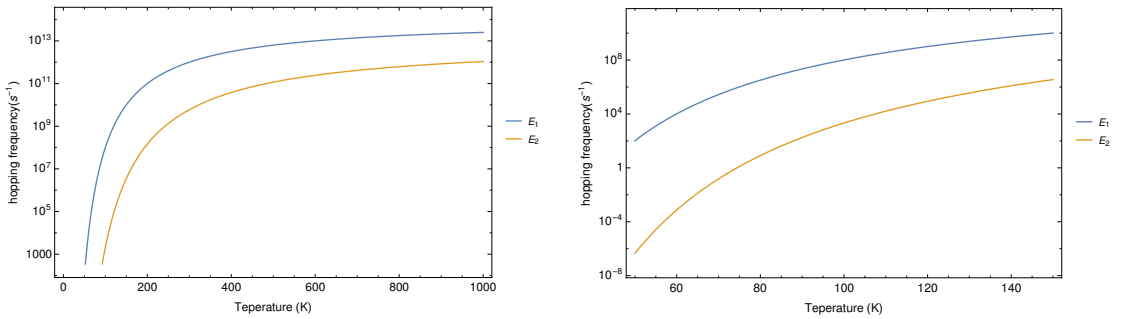

(a) (b)

Figure 14: Hopping frequencies of the B adatom on a log scale against temperature for the path around a N atom (E_1) and the path around a B atom (E_2). In (a) for a temperature range from 0 to 1000 K and in (b) for a temperature range of 50 to 150 K.

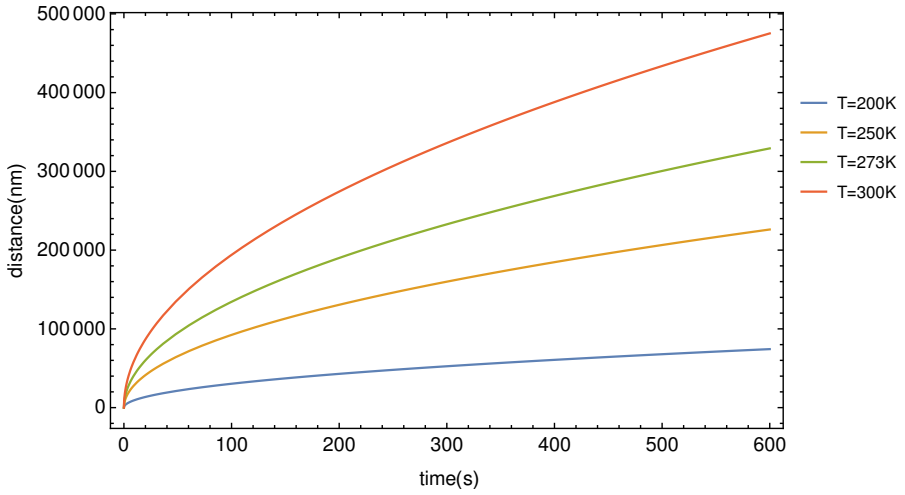

Figure 15: Average distance traveled after a time t for different temperatures T.

5 Conclusion

In this work possible adsorption sites of a boron atom on a boron nitride nanosheet were investigated using DFT calculations. The adsorption site with the highest bond energy was found to be on a hetero bridge with the distance from the B adatom to a N atom about half the distance between the adatom and a B atom. The migration of the adatom on top of the BNNS was also investigated using both the nudged elastic band method and selective dynamics. A diffusion path with whereby diffusion throughout the BNNS is possible was identified and it consists of two distinctive hops. One hop is from a hetero bridge site to a hetero bridge site around a N atom. This hop has a shorter path and lower energy barrier compared to the second hop which is also from a hetero bridge site to a hetero bridge site but around a B atom. With these energy barriers the kinetics of the diffusion were investigated and the calculations showed that diffusion takes place at room temperature. Thus a B adatom is not confined in a certain area on the BNNS.

It was also found that although the NEB method and selective dynamics gave the same energy barrier the calculated values between the two points differed except for the saddle point. Thus the resulting energy curves were different except for the place and height of the peak. Further investigation of which path is accurate is necessary and the application of the NEB method on migration around the B atom to compare the NEB method with the selective dynamics would be interesting as well.

Similar investigation of elements other than boron as adatoms such as nitrogen, carbon and gold could be an interesting follow up study of what was done in this work.

A Appendix

A.1 Convergence

With numerical calculations an important issue is how well converged they are since it determines their accuracy. For the calculations done in this work the parameters that determine the convergence are the energy cutoffs and the k-space sampling. In order to identify the minimum values for these parameters for good convergence some preliminary calculations were done which will be reported here. In order to test the convergence two sets of calculations were done, one for different values for the kinetic cutoff energy of the plane-waves basis set and another for the amount of k-points sampled on the k-mesh. Although the cutoff energy for the augmentation charges also influences the convergence it was not treated as an independent parameter and was always set to 1.4 times the plane-wave energy cutoff.

In order to find a good convergence for the cutoff energy geometry optimization of a 6x6 h-BN supercell was done for different cutoff energies. A high sampling for the k-space was chosen, a k-mesh with a sampling of 12x12x1, for all the calculations in order to measure only the energy cutoff dependence of the convergence. The results would be considered well converged if the energy per atom becomes constant within a range of ± 1 meV compared to the energy per atom calculated at the highest cutoff energy (900 eV). As indicated by Fig. A.1 a minimum cutoff energy of 750 eV is needed to satisfy that condition.

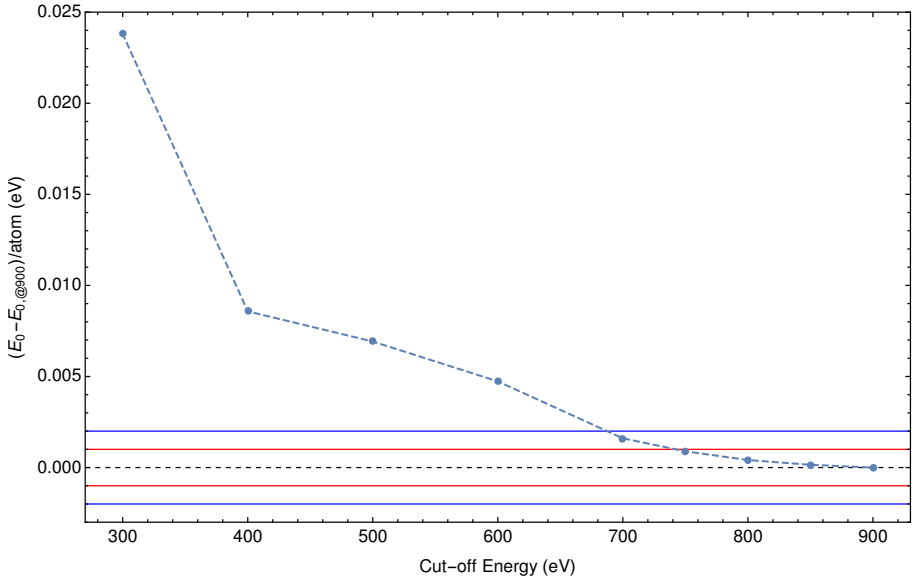

Figure A.1: Calculated energy differences per atom for different cutoff energies of the plane-wave basis set compared to the highest cutoff of 900 eV. All points were calculated with a 12x12x1 k-mesh. The blue dashed line was drawn to guide the eye. The area between the red lines indicates an interval of ±1 meV while the area between the blue lines indicate an ±2 meV interval.

For the k-space sampling a similar approach was used. Geometry optimization was done with a 6x6 h-BN supercell with a high energy cutoff, 900 eV, in order to insure that only the k-space sampling influences convergence. Since the calculations are done on a 2D material the sampling of k-space was done in the following format; axax1, with a being the parameter that was varied for different calculations. As Fig. A.2 indicates a sampling of 2x2x1 satisfies the convergence condition of ±1 eV with respect to that of a sampling of 12x12x1.

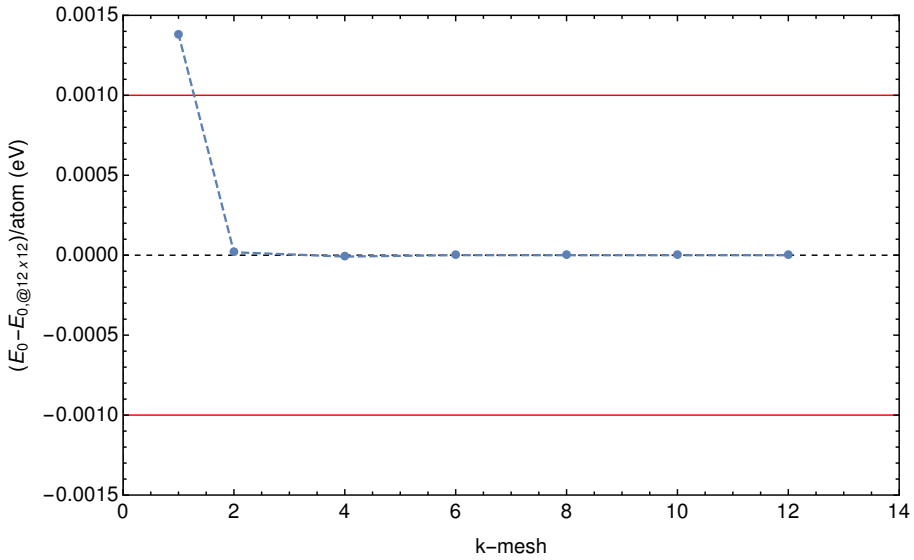

Figure A.2: Calculated energy differences per atom for different k-meshes compared to a k-mesh of 12x12x1. All points were calculated with an energy cutoff of 900 eV. The blue dashed line was drawn to guide the eye. The area between the red lines indicates an interval of ± 1 meV.

A.2 Lattice constant

In order to determine the lattice constant of h-BN preliminary calculations have been done. For different values for the lattice constant geometry optimization was done. The calculations were done with a 1x1 supercell of h-BN with a vacuum layer of at least 20 Å thick between layers to prevent interlayer interaction. The energy cutoff was 750 eV and the k-mesh 12x12x1. As illustrated in Fig. A.3 a lattice constant of 2.51 Å resulted in the lowest energy, this is in agreement with the experimental value[41]. Therefore in all other calculations a lattice constant of 2.51 Å was used.

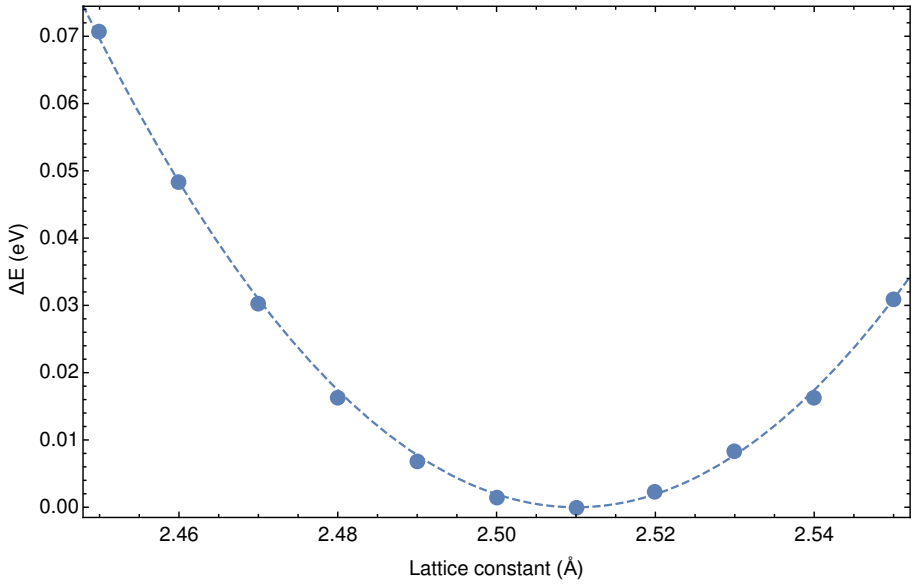

Figure A.3: Calculated energy for different values for the lattice constant. The energy at 2.51 Å has been set as zero and the dashed line is a quadratic fit.

References

[1] Can Ataca, E Aktürk, and Salim Ciraci. Hydrogen storage of calcium atoms adsorbed on graphene: First-principles plane wave calculations. *Physical Review B*, 79(4):041406, 2009.

[2] Alexander A Balandin. Thermal properties of graphene and nanostructured carbon materials. *Nature Materials*, 10(8):569–581, 2011.

[3] Vikas Berry. Impermeability of graphene and its applications. *Carbon*, 62:1–10, 2013.

[4] Saswata Bhattacharya, A Bhattacharya, and GP Das. Anti-kubas type interaction in hydrogen storage on a li decorated bhnh sheet: a first-principles based study. *The Journal of Physical Chemistry C*, 116(5):3840–3844, 2012.

[5] Peter E Blöchl. Projector augmented-wave method. *Physical Review B*, 50(24):17953, 1994.

[6] Max Born and Robert Oppenheimer. Zur quantentheorie der molekeln. *Annalen der Physik*, 389(20):457–484, 1927.

[7] Kieron Burke et al. The abc of dft. *Department of Chemistry, University of California*, 2007.

[8] Kieron Burke and Lucas O. Wagner. Dft in a nutshell. *International Journal of Quantum Chemistry*, 113:96–101, 01/2013 2013.

[9] Yufeng Guo and Wanlin Guo. Insulating to metallic transition of an oxidized boron nitride nanosheet coating by tuning surface oxygen adsorption. *Nanoscale*, 6(7):3731–3736, 2014.

[10] Graeme Henkelman and Hannes Jnsson. Improved tangent estimate in the nudged elastic band method for finding minimum energy paths and saddle points. *The Journal of Chemical Physics*, 113(22):9978–9985, 2000.

[11] Graeme Henkelman, Blas P. Uberuaga, and Hannes Jnsson. A climbing image nudged elastic band method for finding saddle points and minimum energy paths. *The Journal of Chemical Physics*, 113(22):9901–9904, 2000.

[12] P. Hohenberg and W. Kohn. Inhomogeneous electron gas. *Phys. Rev.*, 136:B864–B871, Nov 1964.

[13] Zheng-Hong Huang, Xiaoyu Zheng, Wei Lv, Ming Wang, Quan-Hong Yang, and Feiyu Kang. Adsorption of lead (ii) ions from aqueous solution on low-temperature exfoliated graphene nanosheets. *Langmuir*, 27(12):7558–7562, 2011.

[14] Kabeer Jasuja and Vikas Berry. Implantation and growth of dendritic gold nanostructures on graphene derivatives: electrical property tailoring and raman enhancement. *Acs Nano*, 3(8):2358–2366, 2009.

[15] Erin R. Johnson, Iain D. Mackie, and Gino A. DiLabio. Dispersion interactions in density-functional theory. *Journal of Physical Organic Chemistry*, 22(12):1127–1135, 2009.

[16] R. O. Jones and O. Gunnarsson. The density functional formalism, its applications and prospects. *Rev. Mod. Phys.*, 61:689–746, Jul 1989.

[17] Karen L. Schuchardt, *, Brett T. Didier, Todd Elsethagen, Lisong Sun, Vidhya Gurumoorthi, Jared Chase, Jun Li, , and Theresa L. Windus. Basis set exchange: a community database for computational sciences. *Journal of Chemical Information and Modeling*, 47(3):1045–1052, 2007. PMID: 17428029.

[18] Ji ří Klimeš, David R. Bowler, and Angelos Michaelides. Van der waals density functionals applied to solids. *Phys. Rev. B*, 83:195131, May 2011.

[19] Ji Klime, David R Bowler, and Angelos Michaelides. Chemical accuracy for the van der waals density functional. *Journal of Physics: Condensed Matter*, 22(2):022201, 2010.

[20] W. Kohn and L. J. Sham. Self-consistent equations including exchange and correlation effects. *Phys. Rev.*, 140:A1133–A1138, Nov 1965.

[21] Georg Kresse and Jürgen Furthmüller. Efficient iterative schemes for ab initio total-energy calculations using a plane-wave basis set. *Physical Review B*, 54(16):11169, 1996.

[22] Georg Kresse and Jürgen Hafner. Ab initio molecular dynamics for liquid metals. *Physical Review B*, 47(1):558, 1993.

[23] Nobel Lecture. Electronic structure of matter-wave functions and density functionals, w. kohn. *Rev. Mod. Phys*, 71:1253, 1999.

[24] Changgu Lee, Xiaoding Wei, Jeffrey W Kysar, and James Hone. Measurement of the elastic properties and intrinsic strength of monolayer graphene. *Science*, 321(5887):385–388, 2008.

[25] Chengteh Lee, Weitao Yang, and Robert G. Parr. Development of the colle-salvetti correlation-energy formula into a functional of the electron density. *Phys. Rev. B*, 37:785–789, Jan 1988.

[26] Jae-Hwang Lee, Phillip E Loya, Jun Lou, and Edwin L Thomas. Dynamic mechanical behavior of multilayer graphene via supersonic projectile penetration. *Science*, 346(6213):1092–1096, 2014.

[27] Weiwei Lei, David Portehault, Dan Liu, Si Qin, and Ying Chen. Porous boron nitride nanosheets for effective water cleaning. *Nature Communications*, 4:1777, 2013.

[28] Mel Levy. Universal variational functionals of electron densities, first-order density matrices, and natural spin-orbitals and solution of the v-representability problem. *Proceedings of the National Academy of Sciences*, 76(12):6062–6065, 1979.

[29] Mel Levy. Electron densities in search of hamiltonians. *Phys. Rev. A*, 26:1200–1208, Sep 1982.

[30] Jia Li, Gang Zhou, Ying Chen, Bing-Lin Gu, and Wenhui Duan. Magnetism of c adatoms on bn nanostructures: Implications for functional nanodevices. *Journal of the American Chemical Society*, 131(5):1796–1801, 2009.

[31] Elliott H. Lieb. Density functionals for coulomb systems. *International Journal of Quantum Chemistry*, 24(3):243–277, 1983.

[32] Yi Lin and John W Connell. Advances in 2d boron nitride nanostructures: nanosheets, nanoribbons, nanomeshes, and hybrids with graphene. *Nanoscale*, 4(22):6908–6939, 2012.

[33] Hendrik J Monkhorst and James D Pack. Special points for brillouin-zone integrations. *Physical Review B*, 13(12):5188, 1976.

[34] K. S. Novoselov, A. K. Geim, S. V. Morozov, D. Jiang, Y. Zhang, S. V. Dubonos, I. V. Grigorieva, and A. A. Firsov. Electric field effect in atomically thin carbon films. *Science*, 306(5696):666–669, 2004.

[35] Kostya S Novoselov. Graphene: materials in the flatland (nobel lecture). *Angewandte Chemie International Edition*, 50(31):6986–7002, 2011.

[36] KS Novoselov, D Jiang, F Schedin, TJ Booth, VV Khotkevich, SV Morozov, and AK Geim. Two-dimensional atomic crystals. *Proceedings of the National Academy of Sciences of the United States of America*, 102(30):10451–10453, 2005.

[37] KS Novoselov and AH Castro Neto. Two-dimensional crystals-based heterostructures: materials with tailored properties. *Physica Scripta*, 2012(T146):014006, 2012.

[38] V Ongun Özçelik and S Ciraci. Self-assembly mechanisms of short atomic chains on single-layer graphene and boron nitride. *Physical Review B*, 86(15):155421, 2012.

[39] Amir Pakdel, Yoshio Bando, and Dmitri Golberg. Nano boron nitride flatland. *Chemical Society Reviews*, 43(3):934–959, 2014.

[40] Amir Pakdel, Chunyi Zhi, Yoshio Bando, and Dmitri Golberg. Low-dimensional boron nitride nanomaterials. *Materials Today*, 15(6):256–265, 2012.

[41] W Paszkowicz, JB Pelka, M Knapp, T Szyszko, and S Podsiadlo. Lattice parameters and anisotropic thermal expansion of hexagonal boron nitride in the 10–297.5 k temperature range. *Applied Physics A*, 75(3):431–435, 2002.

[42] John P Perdew, Kieron Burke, and Matthias Ernzerhof. Generalized gradient approximation made simple. *Physical review letters*, 77(18):3865, 1996.

[43] F Schedin, AK Geim, SV Morozov, EW Hill, P Blake, MI Katsnelson, and KS Novoselov. Detection of individual gas molecules adsorbed on graphene. *Nature materials*, 6(9):652–655, 2007.

[44] Daniel Sheppard, Rye Terrell, and Graeme Henkelman. Optimization methods for finding minimum energy paths. *The Journal of Chemical Physics*, 128(13), 2008.

[45] Preeti Singla, Neetu Goel, Sonal Singhal, et al. Boron nitride nanomaterials with different morphologies: Synthesis, characterization and efficient application in dye adsorption. *Ceramics International*, 2015.

[46] Qiao Sun, Zhen Li, Debra J Searles, Ying Chen, Gaoqing Lu, and Aijun Du. Charge-controlled switchable co2 capture on boron nitride nanomaterials. *Journal of the American Chemical Society*, 135(22):8246–8253, 2013.

[47] Qing Tang, Zhen Zhou, and Zhongfang Chen. Molecular charge transfer: a simple and effective route to engineer the band structures of bn nanosheets and nanoribbons. *The Journal of Physical Chemistry C*, 115(38):18531–18537, 2011.

[48] Guo-Hai Yang, Abulikemu Abulizi, and Jun-Jie Zhu. Sonochemical fabrication of gold nanoparticles–boron nitride sheets nanocomposites for enzymeless hydrogen peroxide detection. *Ultrasonics sonochemistry*, 21(6):1958–1963, 2014.

[49] Oleg V Yazyev and Alfredo Pasquarello. Metal adatoms on graphene and hexagonal boron nitride: Towards rational design of self-assembly templates. *Physical Review B*, 82(4):045407, 2010.